The precision of the symmetry in Z-ring placement in Escherichia coli is hampered at critical temperatures

The precision of the symmetry in Z-ring placement in *Escherichia coli* is hampered at critical temperatures

Ramakanth Neeli-Venkata[1], Samuel M.D. Oliveira[1], Leonardo Martins[2], Sofia Startceva[1], Mohamed Bahrudeen[1], Jose M. Fonseca[2], Marco Minoia[1] and Andre S. Ribeiro[1,2, §,*]

Running Head: Precision of the symmetry in Z-ring placement in *E. coli*

Keywords: Z-ring formation and positioning; Critical temperatures; Asymmetry in cell division; Single-cell microscopy; *Escherichia coli*

[1] Laboratory of Biosystem Dynamics, BioMediTech Institute and Faculty of Biomedical Sciences and Engineering, Tampere University of Technology, 33101, Tampere, Finland.
[2] CA3 CTS/UNINOVA. Faculdade de Ciencias e Tecnologia, Universidade Nova de Lisboa, Quinta da Torre, 2829-516, Caparica, Portugal.
[§] Multi-scaled Biodata Analysis and Modelling Research Community, Tampere University of Technology, 33101, Tampere, Finland.
[*] Corresponding author. E-mail: andre.ribeiro@tut.fi, Tel: +358408490736.

Abstract

Cell division in *Escherichia coli* is morphologically symmetric due to, among other, these cells' ability to place the Z-ring at midcell. Studies have reported that, at sub-optimal temperatures, this symmetry decreases at the single-cell level, but the causes remain unclear. Using fluorescence microscopy, we observe FtsZ-GFP and DAPI-stained nucleoids to assess the robustness of the symmetry of Z-ring formation and positioning in individual cells under sub-optimal and critical temperatures. We find the Z-ring formation and positioning to be robust at sub-optimal temperatures, as the Z-ring's mean width, density and displacement from midcell maintain similar levels of correlation to one another as in optimal temperatures. However, at critical temperatures, the Z-ring displacement from midcell is much increased. We show evidence that this is due to enhanced distance between the replicated nucleoids and, thus, reduced Z-ring density, which explains the weaker precision in setting a morphologically symmetric division site. This also occurs in rich media and is cumulative, i.e. combining richer media and critically high temperatures enhances the asymmetries in division, which is evidence that the causes are biophysical. To further support this, we show that the effects are reversible, i.e. shifting cells from optimal to critical, and then to optimal again, reduces and then enhances the symmetry in Z-ring positioning, respectively, as the width and density of the Z-ring return to normal values. Overall, our findings show that the Z-ring positioning in *E. coli* is a robust biophysical process under sub-optimal temperatures, and that critical temperatures cause significant asymmetries in division.

Introduction

In most bacteria, the Z-ring is the main macromolecular structure defining the location of the cell division site [1]. Its formation occurs in parallel with other complex cellular processes, including DNA replication and chromosome segregation [2-4]. The Z-ring consists of cytoskeletal proteins composing FtsZ-protofilaments that serve as a scaffold, along with the FtsA and ZipA linker proteins, for the assembly of the divisome [5-7]. The divisome complex carries out the septal envelope synthesis, followed by the Z-ring constriction. Following the septum formation, the Z-ring disassembles [3,8].

In *Escherichia coli*, the divisome assembly initiates with the polymerization of the tubulin homolog FtsZ, which is organized into a Z-ring, and anchors close to the cytoplasmic membrane that encircles the rod-shaped cell at the center of the major axis [2-4,9]. While evidence suggests that the Z-ring positioning is a stochastic process [10], it is remarkably accurate, allowing cell division to be nearly symmetric [1,11-13].

The Z-ring forms early in the cell cycle and persists without contracting until late in the cell cycle [3]. Studies have reported that Z-rings assume different polymerization

states [14] during the cell cycle. A Z-ring can form and disassemble rapidly (1-3 min for assembly and 1 min for disassembly [15]). This suggests a fast spatial organization of these proteins, when compared to other cellular processes.

Fusing the *ftsz* gene with a green fluorescent protein (FtsZ-GFP) allows visualizing the dynamics of Z-ring formation [14,16]. There are three apparent stages of Z-ring formation [17,18,19]. First, (i) the cells do not exhibit visible rings, and most FtsZ-GFP proteins locate at the one of the cell poles; (ii) next, the cells exhibit two dots at the center, located at opposite sites along the minor axis (open ring state) and, (iii) finally, a distinct band at the cell center appears (closed ring state) [14].

The positioning of the Z-ring along the major cell axis is negatively regulated by (at least) two independent mechanisms: Nucleoid occlusion and the Min system [3,10,20,21]. While the Min system, comprised of three proteins (MinC, MinD, and MinE), inhibits Z-ring assembly at the cell poles [22], nucleoid occlusion, by preventing the Z-ring assembly over the replicated nucleoids by the action of the DNA binding protein, SlmA [23,24], enhances the degree of symmetry of the point of division [10,12]. Their combined action confers cell division in *E. coli* near-symmetry [10].

Temperature is a key environmental variable for bacteria. E.g., *E. coli* growth rates and morphology are temperature-dependent [25,26]. Even the cytoplasm is temperature-dependent, in that, e.g., it acquires glass-like properties due to the enhanced viscosity [27,28].There is evidence of loss of symmetry at non-optimal temperatures [10], which leads to errors/failures in chromosome partitioning [29,30]. Also, recent studies showed that the distance between replicated nucleoids is larger at sub-optimal temperatures [10].

Here, we study how the symmetry in cell division is affected at sub-optimal and, more importantly, critical temperatures, and following temperature shifts. For this, we measure the positioning and morphology of Z-rings. Further, we study whether the effects are reversible and/or cumulative. For this, we use an *E. coli* strain expressing FtsZ-GFP and DAPI staining for nucleoid(s) visualization, and perform single time-point microscopy measurements of cells at optimal, sub-optimal, and critical temperatures.

Methods

Chemicals and Strains

For routine cultures we use Luria-Bertani (LB) medium (10 g of tryptone per liter, 5 g of yeast extract per liter, and 5 g of NaCl per liter), Terrific Broth (TB) (12 g per liter tryptone, 24 g per liter, yeast extract, 0.4% glycerol, and TB salts (KH_2PO_4 and K_2HPO_4)) were used. We also use isopropyl β-D-1-thiogalactopyranoside (IPTG), antibiotic Ampicillin, 4′,6-diamidino-2-phenylindole (DAPI), formaldehyde and agarose for microscopic slide gel preparation and flow cytometry (FC) measurements. All chemicals were purchased from Sigma-Aldrich. We use *E. coli* MG1655-derived strain BS001

expressing *ftsZ-gfp*, under the control of the P_{lac} promoter, incorporated into the chromosome [31] (a kind gift from Daniel O. Daley, Stockholm University, Sweden).

Induction of FtsZ-GFP

Overnight cultures were diluted into fresh LB (or TB) with ampicillin and subcultures were left in the incubator at 37 °C with shaking (250 rpm) until the cells reached the mid-logarithmic phase (OD_{600} ~ 0.25). At this point, FtsZ-GFP expression was induced by 2.5µM IPTG. Cells were then incubated for 30 minutes at 37 °C, prior to shifting to sub-optimal and critical temperatures. Cells were visualized when reaching an OD_{600} ~ 0.4-0.6, depending on the growth condition.

Nucleoid visualization by DAPI staining

DAPI stains nucleoids specifically with little or no cytoplasmic labelling. Induced cells, at appropriate temperatures, were fixed with 3.7% formaldehyde in PBS (pH 7.4) for 30 minutes at RT, followed by washing with PBS to remove excess formaldehyde. The pellets were suspended in PBS, and DAPI (2µg ml^{-1}) was added to the suspension. After incubating for 20 minutes in the dark, cells were centrifuged and washed twice with PBS to remove excess DAPI. Cells were then resuspended in PBS and 5 µL of these samples were placed on 1% agarose gel pad prepared in LB media for microscopy.

Growth Rate measurements

Growth rates were measured by a spectrophotometer (Ultrospec 10; GE Health Care). Cultures were grown overnight with continuous shaking. Next, overnight cultures were diluted into fresh medium to an optical density at 600 nm (OD_{600}) of 0.05. We recorded the OD_{600} values every 30 min for 5 h to obtain growth curves. Results are shown in Supplementary Figure 1. In all cases, FtsZ-GFP expression was induced by adding 2.5µM IPTG to the culture when the cells reached an OD_{600}~0.25. We performed 3 biological replicates per condition. No significant differences were found between them.

Microscopy and Flow-cytometry

After inducing FtsZ-GFP expression for 30 minutes at 37 °C, cells were shifted to specific temperatures (10 °C, 24 °C, 30 °C, 40 °C or 43 °C) or maintained at 37 °C. Next, cells were placed in the incubator (Innova® 40 incubator, New Brunswick Scientific, USA) at the appropriate temperature for 60 minutes, after which they were fixed with 3.7% formaldehyde, followed by DAPI staining and image acquisition.

To subject cells to temperature shifts, cells were grown as described above at 37 °C, followed by induction and image acquisition after 90 minutes. Cells from the same

culture were then shifted to either to 10 °C or 43 °C and left in the incubator for another 60 minutes. Prior to shifting back to 37 °C, 2 ml of these cultures were taken and fixed with 3.7% formaldehyde, followed by DAPI-staining. The sample collection and fixation took less than a minute. Cells that were maintained in the culture were shifted back to 37 °C for 60 minutes and fixed, DAPI-stained and imaged. For these measurements, cells were first placed at the optimal temperature (0^{th} minute) and imaged at the 90^{th} minute. It was followed by a shift at the 90^{th} minute and imaging at the 150^{th}. At this moment (150^{th} minute), we performed the final shift to the optimal temperature and imaged cells for the last time at the 210^{th} minute.

When performing microscopy, cells were placed on 1% agarose gel pad prepared in LB and supplemented with 2.5μM IPTG. Cells were visualized using a Nikon Eclipse (Ti-E, Nikon, Japan) inverted microscope with a C2 confocal laser scanning system using a 100x Apo TIRF (1.49 NA, oil) objective, while DAPI stained nucleoids were observed by epifluorescence microscopy using a mercury lamp with DAPI filter (Nikon). The FtsZ-GFP fluorescence was visualized under the confocal microscope using a 488 nm argon ion laser (Melles-Griot) and a 515/30 nm detection filter. Images were acquired using a medium pinhole, gain 90 and 3.36 μs pixel dwell. The software for image acquisition was NIS-elements (Nikon, Japan). Size of the phase contrast and epifluorescence images was 2560×1920 pixels, in which a pixel corresponds to 0.048 μm, while for confocal images the size of a pixel corresponds to 0.062 μm using a scan resolution of 2048×2048 pixels.

For flow cytometry (FC), cells were prepared as above. At the appropriate moment, the green fluorescence emission (excitation at 488 nm and emission at 509 nm) was measured from the culture using a ACEA NovoCyte Flow Cytometer (ACEA Biosciences Inc., San Diego USA) using blue laser (488 nm) for excitation and the FITC fluorescence detection channel (530/30 nm filter) for emission. Cells were diluted 1:10000 into 1 ml of physiological solution (0.9% NaCl) vortexed for 10 seconds and a total of 50000 cells were test (in 1 run). The flow rate was set at 14 μl/minute, the FSC-H threshold was set at 2000 so that only events (cells) with FSC-H values bigger than the threshold were measured. Three biological replicates were performed (no significant differences were found). We collected data from the Side Scatter Channel Height, SSC-H.

Image Processing and Machine Learning

Cell segmentation from the images was performed using the software “iCellFusion” [32] and “CellAging” [33], which perform automatic segmentation from phase contrast images (Figure 1A), but allow manual corrections for increased accuracy. A 2-D affine geometric transformation [34] is used to transform epifluorescence images (Figure 1B) into the same resolution space as confocal images (Figure 1C). Nucleoid(s) segmentation is performed as in [28], using a 2-dimensional Gaussian approximation. The number of nucleoids in a

cell is counted by the Gradient Path Labelling (GPL) algorithm [35], followed by manual corrections. A similar algorithm is used to automatically locate the boundaries of the Z-ring by selecting a fluorescence level threshold for each cell and separate the FtsZ-GFP signal from the background [36,37,38]. This was only applied to cells selected by machine learning to be in the 3rd stage of Z-ring formation [19].

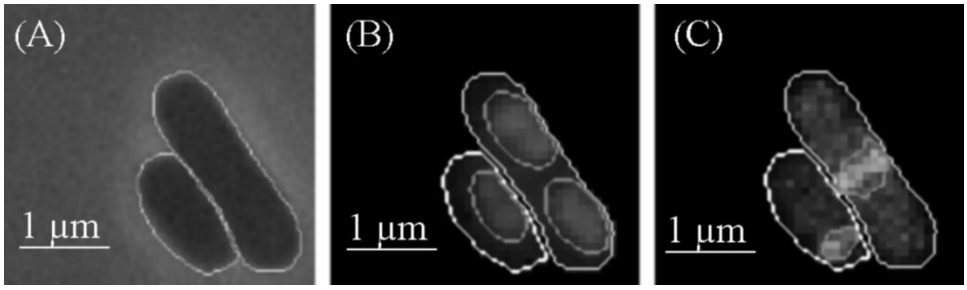

Figure 1. Example images of cells at 37 °C. (A) Phase-Contrast image with cell segmentation. (B) DAPI-stained nucleoids visualized by Epifluorescence microscopy. (C) Confocal images with FtsZ-GFP labelled rings with cell segmentation and Z-ring segmentation (light grey line) based on threshold selection.

To perform automatic selection of the stage of Z-ring formation, after image processing, we use Regularized Multinomial Logistic Regression (RMLR), trained to distinguish the stages of the Z-ring formation [19] (accuracy of 80% or higher). Example images of a cell in the three stages of Z-ring formation are shown in Figure 2.

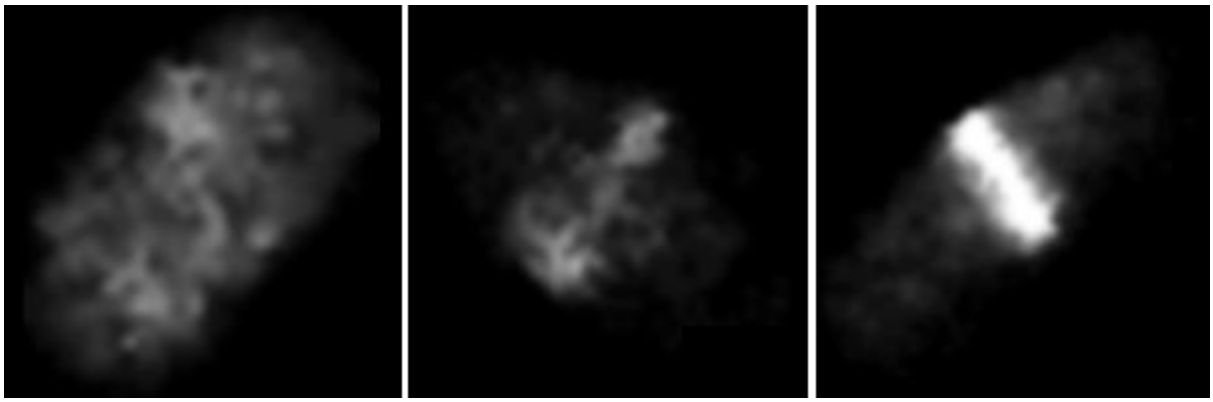

Figure 2. Example confocal microscopy images of cells expressing FtsZ-GFP in each of the three stages of Z-ring formation. Left to right: i) stage 1: most FtsZ-GFP at the poles; ii) stage 2: FtsZ-GFP distributed as an ‘open ring’; and (C) stage 3: FtsZ-GFP distributed as a ‘closed ring’ [14].

Results and Conclusions

To study how temperature affects the formation and positioning of the Z-ring, we use *E. coli* strain MG1655, modified to express fluorescent FtsZ–GFP (Methods). The ratio of native FtsZ:FtsZ–GFP is ~60:40 [39]. Induction with IPTG in the concentrations used here (and up to 10 μM), do not affect cell growth or morphology [39,40], in that the cells exhibit a division rate and behaviour similar to the parental strain. Unless stated otherwise, all results are from cells imaged by microscopy.

Growth, nucleoid partitioning and Z-ring formation at sub-optimal and critical temperatures

We first assessed cell growth rates in each temperature and media condition analysed here. In no condition, the cells exhibited lethality, although at 10°C almost no growth was visible (Supplementary Figure S1). Also, in no condition did the cells' morphology exhibit anomalies.

Cells were kept at the appropriate temperature for 90 minutes, prior to fixation and DAPI staining, after which they were imaged (Methods). From the images, cells were segmented and their stage of Z-ring formation was classified [19][49][50] (Methods). The fraction of cells with 2 nucleoids and in stage 3 was found to be between 6-13%, depending on the growth condition (Table 1), in agreement with previous studies [51].

Table 1. Temperature-dependence of the fraction of cells exhibiting Z-rings in stage 3 of formation, following nucleoid splitting. Shown are the temperature and number of cells analyzed with 2 nucleoids and with 2 nucleoids and a Z-ring in the stage 3 of formation. The second column also informs on the fraction of cells with 2 nucleoids (in %, relative to the number of cells observed). The last column informs on the fraction of cells with 2 nucleoids that also have a Z-ring in the stage 3 of formation (in % relative to the number of cells with 2 nucleoids). Measurements were conducted in LB media.

T (˚C)	No. cells observed	No. cells with 2 nucleoids	No. cells with 2 nucleoids and with a Z-ring in the stage 3 of formation
43	1466	169 (12%)	113 (67%)
40	1821	135 (7%)	115 (85%)
37	1161	153 (13%)	133 (94%)
30	1784	203 (11%)	138 (91%)
24	1464	138 (9%)	121 (88%)
10	1989	405 (20%)	183 (45%)

From Table 1, at 37 °C (control), the fraction of cells with 2 nucleoids and the fraction of cells with 2 nucleoids and the Z-ring in stage 3 are similar (i.e. only 6% of the cells with 2 nucleoids do not have the Z-ring in stage 3), suggesting that, at 37 °C, when nucleoid partitioning occurs, so does Z-ring formation. Meanwhile, the higher the

deviation from the optimal temperature, the smaller is the fraction of cells with partitioned nucleoids that also have a Z-ring in stage 3 (column 4 in Table 1), suggesting that temperature deviations from the optimal condition affect, by different degrees, the ability of cells to partition the nucleoid and to reach stage 3 of Z-ring formation (with the latter process being more affected).

Past studies [41] suggested that, following nucleoid replication, the two resulting nucleoids differ in density from the original nucleoid. We confirmed this by measuring the intensity of the DAPI fluorescence distributions along the major cell axis (Figure 3).

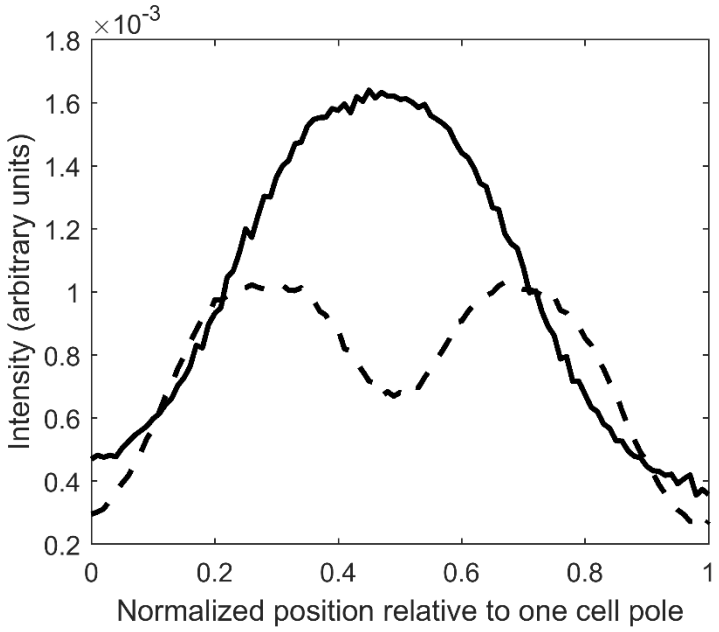

Figure 3. Distributions of fluorescence intensity of DAPI-stained cells along the major axis (averaged over all cells) for cells with one nucleoid (thick line, 112 cells) and with two nucleoids (dashed line, 109 cells). Cell lengths along the major axis are normalized relative to the position of one of the poles.

Given this, one can predict that cells with 2 nucleoids may differ in overall granularity from those with 1 nucleoid. We assessed this by Flow-cytometry (Side Scatter Channel Height, SSC-H) [42]. We use the SSC-H measurements as a means to assess (independently), the expected fraction of cells at 37 °C that are close to division at any given time in the control condition. Further, note from Table 1 that, in this condition, there is a 94% probability that cells with 2 nucleoids will also have a Z-ring in stage 3. Thus, we also use this as a means to assess the maximum expected fraction of cells with 2 nucleoids and a Z-ring in stage 3. Results from flow-cytometry are shown in Figure 4.

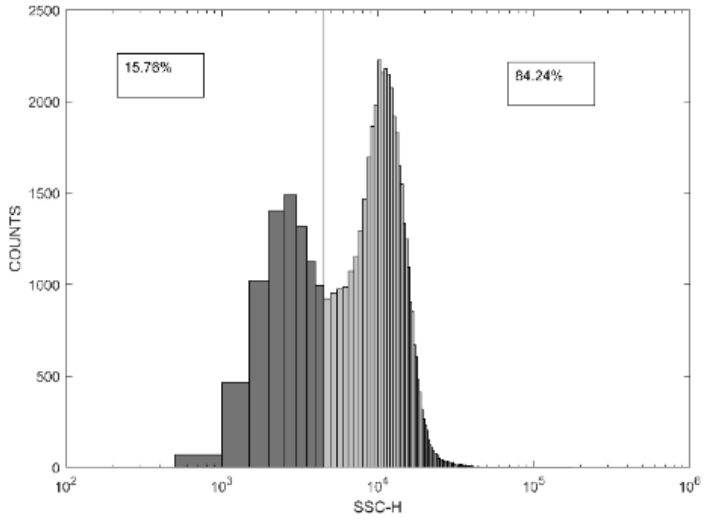

Figure 4. Distributions of the number of cells with given values of SSC-H as obtained by flow-cytometry of cells grown in the control condition. X-axis in log-scale. Sample size of 50 000 cells.

From Figure 4, there are two distinct cell populations, in that ~16% of the cells exhibit lower values of SSC-H (corresponding to lower granularity, likely due to having 2 nucleoids since this is the percentage of cells shown in Microscopy to be dividing at any given moment). Given that 94% of these cells should have a Z-ring in stage 3 of formation as seen by microscopy, we infer that, according to the single-cell values of SSC-H, ~14% of the cells should have 2 nucleoids and a Z-ring in stage 3. These results are in accordance with the results from fluorescence microscopy, extracted by image analysis and machine learning (12.4%, Table 1). We conclude that the image analysis methods applied to the microscopy data are accurate in detecting cells with two nucleoids and FtsZ-GFP rings in stage 3.

Finally, overall, from Table 1, we find that temperature affects the ability of cells to reach the stage 3 of Z-ring formation. Given the increasing difference (as temperature differs more from the control condition) between the fraction of cells with 2 nucleoids and the fraction of cells with 2 nucleoids and the Z-ring formed, we conclude that the ability of the Z-ring to reach stage 3 of formation is more affected by sub-optimal and critical temperatures than the ability of nucleoid partitioning.

Next, to explain this, we investigate which biophysical properties of the Z-ring in stage 3 change with temperature, within the range of sub-optimal temperatures.

Z-ring distance to midcell and density are robust within sub-optimal temperatures

First, we study the effects of temperature on the Z-ring's location along the major cell axis and density, when in stage 3, in the range of sub-optimal temperatures. For this, we imaged cells that were grown for 90 minutes at 24°C, 30°C, 37°C (control), and 40°C. Next, we selected from the images (Methods) cells with 2 nucleoids and a Z-ring in stage 3 for further analysis. No cells with more than 2 nucleoids were observed. Cells with 2 nucleoids without a Z-ring in stage 3 were excluded from the analysis.

From the images, we extracted from each cell the smallest distance between the nucleoids' borders (d_{nuc}), the Z-ring width (*w*), the Z-ring displacement from midcell (d_{mid}), and the Z-ring's density (ρ) (estimated from the total brightness of the FtsZ-GFP proteins relative to the width of the Z-ring along the major cell axis). Results are shown in Table 2, relative to the control (37°C).

Table 2. Number of cells analyzed, mean minimum distance between replicated nucleoids (d_{nuc}), mean Z-ring width along the major cell axis (*w*), mean Z-ring density (ρ) of the Z-ring in individual cells, and mean displacement of the Z-ring center along the main cell axis from midcell (d_{mid}) in each condition. The values are relative to the control condition (37°C).

T (˚C)	No. cells	d_{nuc}	w	ρ	d_{mid}
24	121	1.2	1.3	0.8	1.5
30	138	1.2	1.2	0.8	1.4
37	144	1	1	1	1
40	115	1.1	1.2	0.6	1.5

From Table 2, in agreement with [10], d_{nuc} gradually increases as temperature gradually differs more from 37°C. Also, *w* increases as d_{nuc} increases, in agreement with past studies suggesting that the nucleoids location and/or size affect the symmetry in localization of the point of cell division along the major cell axis of the mother cell [10,30,43,44], as well as the location of, e.g., protein aggregates and the serine chemoreceptor [41,45,46].

This gradual increase in *w* at sub-optimal temperatures is also in agreement (and explains) with the gradually lower values of ρ. Further, this decrease in ρ can explain the increased loss of centrality of the Z-ring center along the major cell axis, d_{mid}.

Overall, we conclude that, at sub-optimal temperatures, the asymmetry in division in *E. coli* increases (as reported in [10]), due to ρ decreasing and d_{mid} increasing, which is expected to diminish the cell's efficiency in placing the Z-ring center at midcell. Nevertheless, note that, within the range of sub-optimal temperatures, overall, while exhibiting small differences when compared to the optimal condition, the formation and

symmetric positioning of the Z-ring appears to remain robust, in that the deviations relative to the control are small and gradual.

To illustrate this, for each condition, we obtained the ratios $\frac{d_{mid}}{d_{nuc}}$, $\frac{w}{d_{nuc}}$ and $\frac{w}{d_{mid}}$ at each temperature. These ratios evaluate, respectively, whether the mean displacement of the Z-ring is consistent with the mean distance between nucleoids, whether the mean width of the Z-ring is consistent with the mean distance between nucleoids, and whether the mean width of the Z-ring is consistent with the displacement of the Z-ring. In other words, if these ratios can be distinguished, in a statistical sense, between conditions, it would be indicative that the symmetry in cell division, based on the nucleoids positioning and subsequent Z-ring formation and positioning, is not being robust to the changing temperatures. Results are shown in Table 3.

Table 3. Ratios between Z-ring displacement (d_{mid}) and distance between the replicated nucleoids (d_{nuc}), between Z-ring width along the major cell axis (*w*) and d_{nuc}, and between *w* and d_{mid}. The values are relative to the control condition (37°C).

T (˚C)	$\frac{w}{d_{nuc}}$	$\frac{d_{mid}}{d_{nuc}}$	$\frac{w}{d_{mid}}$
24	1.1	1.2	0.9
30	1.0	1.2	0.9
37	1	1	1
40	1.1	1.4	0.8

To make use of the ratios in Table 3 as a means to assess whether size and location of the nucleoids and Z-ring remain consistent to each other for the temperature range of 24 ˚C to 40 ˚C, we performed tests of statistical significance (Kolmogorov-Smirnov tests, i.e. KS-tests) between their values at the various conditions (Supplementary Table 1).

From Supplementary Table 1, all p-values from the KS-tests between each pair of conditions in the range of sub-optimal temperatures inform that no ratios' values can be distinguished in a statistical sense between any pair of temperature conditions. This confirms that d_{nuc}, w, and d_{mid} change gradually with temperature in a predictable and correlated manner, i.e., no 'sharp' changes are observed in this range of temperatures. In that sense, the observations suggest that the Z-ring formation and positioning remain robust at sub-optimal temperatures. Next, we investigate if this robustness is also observed at critically high and low temperatures.

Z-ring localization relative to midcell is sensitive to critical temperatures

Using the methods above, we investigated the effects of critical temperatures on the formation and positioning of the Z-ring. For this, we imaged cells grown for 90 minutes at 10 °C and at 43 °C. These temperatures are considered 'critical' since several phenomena can occur at these

temperatures (e.g increased cytoplasm viscosity [28] and protein aggregation [47]). These could affect significantly the formation and positioning of the Z-ring. Results in Table 4 confirm this.

Table 4. Number of cells analyzed, mean minimum distance between replicated nucleoids (d_{nuc}), mean Z-ring width along the major cell axis (*w*), mean Z-ring density (ρ) of the Z-ring in individual cells, and mean displacement of the Z-ring from midcell (d_{mid}) in each condition. The values are relative to the control condition (37°C).

T (˚C)	No. cells	d_{nuc}	w	ρ	d_{mid}
10	183	1.4	1.3	0.6	2.1
37	144	1	1	1	1
43	113	1.2	1.2	0.6	2.0

From Table 4, and compared to the results in Table 2, we observe that the Z-rings biophysical properties and the distance between nucleoids appear to differ significantly from the control condition (i.e. significantly more than the sub-optimal conditions). Namely, both at 10 °C and 43 °C, d_{mid} is double the value in the control condition. Again, we calculated the ratios $\frac{w}{d_{nuc}}$, $\frac{d_{mid}}{d_{nuc}}$ and $\frac{w}{d_{mid}}$ at each temperature to assess these differences relative to the control (Table 5).

Table 5. Ratios between Z-ring displacement (d_{mid}) and the distance between the two replicated nucleoids (d_{nuc}), between Z-ring width along the major cell axis (w) and d_{nuc}, and between *w* and d_{mid}. Values are relative to the control condition (37°C).

T (˚C)	$\frac{w}{d_{nuc}}$	$\frac{d_{mid}}{d_{nuc}}$	$\frac{w}{d_{mid}}$
10	0.9	1.5	0.6
37	1	1	1
43	1	1.6	0.6

From Table 5, compared to Table 3, we see more significant differences in the values of these ratios when compared to the control. To assert that these differences are significant, we performed tests of statistical significance between these ratios for all pairs of conditions. Results in Supplementary Table 1 confirm that the values of the ratios can be distinguished in a statistical sense between any pair of temperature conditions considered in Table 5 (which does not occur in the regime of sub-optimal temperatures shown in Table 3).

From this, we conclude that, at the critical temperatures tested here, the process of Z-ring formation and positioning at stage 3 loses its strict relationship with the positioning of the replicated nucleoids. Further, we find that these ratios also differ (in a statistical sense, i.e. the p-

values are smaller than 0.01) between 10 °C and 43 °C, which suggests that the causes for the loss of robustness of Z-ring formation and positioning at these critical temperatures might differ.

Next, we investigate whether the observed phenomenon is cumulative (as expected from being of a biophysical nature), i.e., can be enhanced or reduced by the combination of two independent external factors.

Media richness and critically high temperatures have a cumulative effect on the degree of asymmetry of the Z-ring positioning

Previous studies have shown that rich media causes an increase of the average distance between replicated nucleoids, prior to cell division [46]. One reason for this might be that, e.g., in TB media at 37 °C, replicated nucleoids segregate much before cell division than in LB media [48]. Likely due to this, the gap between the newly formed nucleoids is also, on average, 10% larger in TB media than in LB media [44]. We thus hypothesized that combining TB media and critically high temperatures (43 °C) should cause higher morphological asymmetries in division than if cells are in TB media at 37 °C and than if cells are in LB media at 43 °C. Results from these measurements are shown in Table 6 and confirm these predictions.

Table 6. Number of cells analyzed, mean minimum distance between replicated nucleoids (d_{nuc}), mean Z-ring width along the major cell axis (w), and mean displacement of the Z-ring from midcell (d_{mid}) in each condition. The values are relative to the control condition (LB media at 37°C).

Condition	No. cells	d_{nuc}	w	d_{mid}
37 °C LB	144	1	1	1
43 °C LB	113	1.2	1.2	2.0
37 °C TB	169	1.4	1.2	1.7
43 °C TB	120	1.7	1.3	2.2

From Table 6, d_{nuc}, w, and d_{mid}, are all maximal in cells at 43 °C in TB media. We thus conclude that the effects of critically high temperatures and rich media are cumulative, which is consistent with the loss of symmetry in the positioning of the Z-ring at non-optimal conditions being a biophysical phenomenon, rather than being due to a cellular response mechanism. If so, the effects of placing the cells in these conditions should be reversible, once the cells are placed again in optimal conditions.

Next, we test whether this phenomenon is reversible, at least partially.

The effects of Z-ring displacement at critical temperatures are reversible

We assessed if the observed displacements in the Z-ring positioning are reversible. i.e., do cells subject to critical temperatures, when changed to optimal temperatures, regain the ability to undergo symmetric division by positioning the Z-ring at the geometric cell center? We tested this

by shifting cells from the control condition (37 °C) to critical conditions (10 °C or 43 °C), and then back to the control condition (37 °C). Results are shown in Tables 7 and 8.

Table 7: Reversibility of Z-ring displacement following two temperature shifts: from 37 °C to 43 °C and then from 43 °C to 37 °C. The values of d_{nuc}, *w* and d_{mid} are relative to the control condition (37 °C at the start of the measurements). Cells are kept in each of the three conditions for 60 min., followed by sample collection, fixation, observation, and then a temperature shift.

Condition	No. cells	d_{nuc}	*w*	d_{mid}
37 °C	144	1	1	1
Shift to 43 °C	133	1.09	1.04	2.13
Shift to 37 °C	142	1.02	1.02	1.32

Table 8: Reversibility of Z-ring displacement following two temperature shifts: from 37 °C to 10 °C and then from 10 °C to 37 °C. The values of d_{nuc}, *w* and d_{mid} are relative to the control condition (37 °C at the start of the measurements). Cells are kept in each of the three conditions for 60 min., followed by sample collection, fixation, observation, and then a temperature shift.

Condition	No. cells	d_{nuc}	*w*	d_{mid}
37 °C	143	1	1	1
Shift to 10 °C	144	1.46	1.08	2.15
Shift to 37 °C	160	1.12	1.04	1.31

From Tables 7 and 8, while the parameters in the last moment of data acquisition do not exhibit complete reversibility to their initial values (in agreement with observations reported in [51]), a partial reversibility is visible in all three ratios analyzed. This supports the conclusion that the observed phenomenon is biophysical.

Discussion

We studied the robustness of the process of Z-ring formation and positioning when at sub-optimal and critical temperatures in *E. coli*. Both the formation and positioning of the Z-ring were found to be hampered, particularly at critically high and low temperatures.

We observed that the Z-ring formation and positioning are less robust to sub-optimal and critical temperatures than the process of nucleoid(s) partitioning. The robustness of these two processes to the temperature shifts are expected to differ, since the elements involved in the Z-ring formation and positioning [1-5,10,13,15,20,21], and those involved in nucleoid partitioning (see e.g. [52]) differ. In the future, it would be of interest to investigate which elements associated to the Z-ring formation and positioning are “responsible” for this weaker robustness to temperature shifts.

We found Z-ring formation and positioning to be robust within the range of sub-optimal temperatures in that, while the symmetricity in Z-ring positioning (and subsequent cell division) is weaker at the single-cell level, the quantitative relationships (ratios) between the various parameters expected to affect this symmetry do not differ significantly between conditions, in a statistical sense.

However, these ratios exhibit statistically significant differences between critically high and low temperatures tested here when compared to the control condition. We expect this to be the result of wider distance between nucleoids that results in a less dense Z-ring, which increases significantly the stochasticity of the location where the Z-ring will form relative to midcell.

An additional reason why the Z-ring positioning becomes particularly hampered at critically high temperatures might be the hampering of the nucleoid's ability to efficiently exclude FtsZ protofilaments, as some of the proteins responsible for the exclusion may also have weakened functionality in these conditions (e.g. SlmA [23,24]). Meanwhile, at critically low temperatures, the increased viscosity of the cytoplasm [27,28] is expected to play a role in the loss of efficiency as well.

Importantly, we provided evidence that the degree of symmetry in cell division in *E. coli* is, to a great extent, supported by a biophysical phenomenon. First, we showed that the effects of multiple different-than-the-control conditions are cumulative (e.g. combining richer media and critically high or low temperatures causes higher asymmetries in division than when imposing only one of these differences compared to the control). Second, we showed that the effects of placing cells in non-optimal conditions are reversible.

Overall, our findings indicate that the Z-ring positioning in *E. coli* is a robust biophysical process under sub-optimal temperatures, and that critical temperatures cause significant asymmetries in division. We conclude that the degree of symmetry in cell division in *E. coli* is likely of importance, since mechanisms evolved to ensure this symmetry within the range of sub-optimal temperatures. This is expected, given that, in single-celled organisms, defects in cell size are usually detrimental.

However, no biological mechanisms appear to have evolved in *E. coli* capable of sustaining the same levels of efficiency at critically high or low temperatures. One possible reason is that these mechanisms would be too costly (e.g. energetically). We hypothesize that this lack of an energy-costly mechanism is a better option for the perpetuation of the population, at the expense of some individuals when encountering, at sporadic moments, critical conditions.

In a previous study [10], we showed that the degree of morphological symmetry in cell division in *E. coli* is temperature dependent. We also showed that there was a clear

correlation between the occurrence of asymmetries in the location of point of cell division relative to midcell with a larger distance between the nucleoids prior to division. At sub-optimal temperatures, this distance was, on average, larger (by ~7% at 24 ºC and 42 ºC when compared to 37 ºC), explaining the larger and more frequent morphological asymmetries in cell division. The results shown here explain this, in that the effects of sub-optimal and critical temperatures on the behaviour of the Z-rings are consistent with their effects on the degree and rate of occurrence of morphological asymmetries in cell division reported in [10]. Namely, we argue that our observations (e.g. wider distances between nucleoids resulting in wider and more displaced Z-rings at non-optimal conditions) and those reported in [10] are both consistent with a nucleoid exclusion phenomenon (see e.g. [10,45,46,53]) being one of the most contributing factors to the localization and shape of the Z-ring and, thus, of the point of cell division in *E. coli*. Such phenomenon of nucleoid exclusion is already well known to be of importance in localization of plasmids [54,55] and other large complexes [45,56]. Future studies focusing on the role of specific proteins and other features of the nucleoid responsible for this exclusion phenomena may provide additional evidence for this.

In this regard, it will be of interest to observe the behaviour of the other proteins composing the divisome [1-5], under the conditions studied here. This will allow answering, among other questions, whether the observed levels of displacement in Z ring position is also observed in the positioning of other divisome constituents, such as ZapA, ZapB and ZipA. We expect this to occur, given that the final outcome, i.e. the sizes of the daughter cells was shown to exhibit higher asymmetry levels at non-optimal temperatures [10].

Author Contributions

RN-V performed most experiments. SO, LM, MB and SS performed the image and data analysis. MM performed the Flow-cytometry experiments. ASR and RN-V conceived the study and wrote the manuscript, which was revised by all authors.

Acknowledgments

Work supported by Tampere University of Technology President's Graduate Programme (R.N-V, S.S. and M.B), Portuguese Foundation for Science and Technology FCT/MCTES (SFRH/BD/88987/2012 to L.M.), Finnish Academy of Science and Letters (SO), Academy of Finland (295027 to A.S.R.), Academy of Finland Key Project Funding (305342 to A.S.R.), and Jane and Aatos Erkko Foundation (610536 to A.S.R.). The funders had no role in study design, data collection and analysis, decision to publish, or preparation of the manuscript. The authors declare that they have no conflict of interest.

References

[1] Yu X C and Margolin W 1999 FtsZ ring clusters in min and partition mutants: role of both the Min system and the nucleoid in regulating FtsZ ring localization *Mol. Microbiol.***32** 315–26

[2] Margolin W 2005 FtsZ and the division of prokaryotic cells and organelles *Nat. Rev. Mol Cel. Biol.* **6** 862–71

[3] Adams DW and Errington J 2009 Bacterial cell division: assembly, maintenance and disassembly of the Z ring Nat.Rev. Microbiol. 7 642–53

[4] Lutkenhaus J, Pichoff S and Du S 2012 Bacterial cytokinesis: From Z ring to divisome *Cytoskeleton* **69** 778–90

[5] Errington J, Daniel RA and Scheffers DJ 2003 Cytokinesis in bacteria *Microbiol. and Mol. biol. Rev.* **67** 52–65

[6] Goehring NW and Beckwith J 2005 Diverse paths to midcell: assembly of the bacterial cell division machinery *Curr. Biol.* **15** 514–26

[7] Harry E, Monahan L and Thompson L 2006 Bacterial cell division: the mechanism and its precison *Int. rev. cyt.* **253** 27–94

[8] Addinall SG, Bi E and Lutkenhaus J 1996 FtsZ ring formation in fts mutants *J. Bacteriol.* **178** 3877–84

[9] Bi E and Lutkenhaus J 1991 FtsZ ring structure associated with division in Escherichia coli *Nature* **354** 161–64

[10] Gupta A, Lloyd-Price J, Oliveira SMD, Yli-Harja O, Muthukrishnan AB and Ribeiro AS 2014 Robustness of the division symmetry in Escherichia coli and functional consequences of symmetry breaking *Phys. Biol.* **11** 66005

[11] Hiraga S, Niki H, Ogura T, Ichinose C, Mori H, Ezaki B, and Jaffe A 1989 Chromosome Partitioning in Escherichia coli: Novel Mutants Producing Anucleate Cells. *J. of Bacteriol.* **171** 1496-1505

[12] Guberman JM, Fay A, Dworkin J, Wingreen NS and Gitai Z 2008 PSICIC: Noise and asymmetry in bacterial division revealed by computational image analysis at sub-pixel resolution *PLoS Comp. Biol* **4** e1000233

[13] Männik J, Wu F, Hol F J H, Bisicchia P, Sherratt D J, Keymer J E and Dekker C 2012 Robustness and accuracy of cell division in Escherichia coli in diverse cell shapes *Proc. Natl. Acad. Sci. USA* **109** 6957–62

[14] Ma X, Ehrhardt DW and Margolin W 1996 Colocalization of cell division proteins FtsZ and FtsA to cytoskeletal structures in living Escherichia coli cells by using green fluorescent protein *Proc. Natl. Acad. Sci. USA* **93** 12998–3003

[15] Addinall SG, Cao C and Lutkenhaus J 1997 Temperature shift experiments with an ftsZ84(Ts) strain reveal rapid dynamics of FtsZ localization and indicate that the Z ring is required throughout septation and cannot reoccupy division sites once constriction has initiated *J. Bacteriol.* **179** 4277–84

[16] Galli E and Gerdes K 2012 FtsZ-ZapA-ZapB interactome of Escherichia coli *J. Bacteriol.* **194** 292–302

[17] Tsukanov R, Reshes G, Caramon G, Friedrich EF, Gov NS, Fishov I, Feingold M 2011 Timing of Z-ring localization in Escherichia coli *Phys. Biol.*, **8** 066003

[18] Rueda S, Vicente M and Mingorance J 2003 Concentration and assembly of the division ring proteins FtsZ, FtsA, and ZipA during the Escherichia coli cell cycle *J. Bacteriol.* **185** 3344–51

[19] Zare M, Neeli-Venkata R, Martins L, Peltonen S, Ruotsalainen U, and Ribeiro AS 2017 Automatic classification of Z-ring formation stages at the single cell level in Escherichia coli by Machine Learning. 4th International Conference on Bioimaging (Biomaging 2017), Porto, Portugal

[20] Rothfield L, Taghbalout A and Shih YL 2005 Spatial control of bacterial division-site placement *Nat. Rev. Microbiol.* **3** 959–68

[21] Lutkenhaus J 2007 Assembly dynamics of the bacterial MinCDE system and spatial regulation of the Z ring *Ann. rev. Biochem.* **76** 539–62

[22] Raskin DM and de Boer PA 1999 Rapid pole-to-pole oscillation of a protein required for directing division to the middle of Escherichia coli *Proc. Natl. Acad. Sci. USA* **96** 4971–6

[23] Cho H, McManus HR, Dove SL and Bernhardt TG 2011 Nucleoid occlusion factor SlmA is a DNA-activated FtsZ polymerization antagonist *Proc. Natl. Acad. Sci. USA* **108** 3773–78

[24] Tonthat NK, Arold ST, Pickering BF, Van Dyke MW, Liang S, Lu Y, Beuria TK, Margolin W and Schumacher MA 2011 Molecular mechanism by which the nucleoid occlusion factor, SlmA, keeps cytokinesis in check *EMBO J.* **30** 154–64

[25] Farewell A and Neidhardt FC 1998 Effect of Temperature on In Vivo Protein Synthetic Capacity in Escherichia coli *J. Bacteriol* **180** 4704-10

[26] Shehata TE and Marr AG 1975 Effect of Temperature on the Size of Escherichia coli Cells *J. Bacteriol* **124** 857-62

[27] Parry BR, Surovtsev IV, Cabeen MT, O'Hern CS, Dufresne ER, Jacobs-Wagner C 2014 The bacterial cytoplasm has glass-like properties and is fluidized by metabolic activity *Cell* **156** 183–94

[28] Oliveira SMD, Neeli-Venkata R, Goncalves NSM, Santinha JA, Martins L, Tran H, Mäkelä J, Gupta A, Barandas M, Häkkinen A, Lloyd-Price J, Fonseca JM and Ribeiro AS 2016 Increased cytoplasm viscosity hampers aggregate polar segregation in Escherichia

coli *Mol. Microbiol.* **99** 686–99

[29] Weart RB, Lee AH, Chien AC, Haeusser DP, Hill NS and Levin PA 2007 A Metabolic Sensor Governing Cell Size in Bacteria *Proc. Natl. Acad. Sci. USA* **130** 335-47

[30] Männik J and Bailey MW 2015 Spatial coordination between chromosomes and cell division proteins in Escherichia coli *Front. in microbiol.* **6** 306

[31] Söderström B, Mirzadeh K, Toddo S, von Heijne G, Skoglund U and Daley DO 2016 Coordinated disassembly of the divisome complex in Escherichia coli *Mol. Microbiol.* **101** 425–38

[32] Santinha J, Martins L, Häkkinen A, Lloyd-Price J, Oliveira SMD, Gupta A, Annila T, Mora A, and Ribeiro AS and Fonseca JM 2015 iCellFusion – a Tool for Fusion of Time-lapsed Multimodal Microscopy images *Biomedical Image Analysis and Mining Techniques for Improved Health Outcomes*, IGI Global, USA, 71-99

[33] Häkkinen A, Muthukrishnan AB, Mora A, Fonseca JM, and Ribeiro AS 2013 CellAging: A tool to study segregation and partitioning in division in cell lineages of Escherichia coli *Bioinformatics* **29** 1708-09

[34] Sonka M, Hlavac V, and Boyle R 2014 Image processing, Analysis, and Machine Vision Cengage Learning, Massachusetts, USA

[35] Mora AD, Vieira PM, Manivannan A and Fonseca JM 2011 Automated drusen detection in retinal images using analytical modelling algorithms *Biomed. Eng. Online* **10** 59

[36] Häkkinen A and Ribeiro AS 2015 Estimation of GFP-tagged RNA numbers from temporal fluorescence intensity data *Bioinformatics* **31** 69-75

[37] Oliveira SMD*, Häkkinen A*, Lloyd-Price J, Tran H, Kandavalli V, and Ribeiro AS 2016 Temperature-Dependent Model of Multi-Step Transcription Initiation in Escherichia coli Based on Live Single-Cell Measurements *PLoS Comput Biol* **12** e1005174

[38] Goncalves NSM, Startceva S, Palma CSD, Bahrudeen MNM, Oliveira SMD and Ribeiro AS 2017. Temperature-dependence of the single-cell kinetics of transcription activation in Escherichia coli *Phys. Biol.* **15** 026007

[39] Söderström B, Skoog K, Blom KH, Weiss DS, von Heijne G and Daley DO 2014 Disassembly of the divisome in Escherichia coli: evidence that FtsZ dissociates before compartmentalization *Mol. Microbiol.* **92** 1-9

[40] Lloyd-Price J, Startceva S, Kandavalli V, Chandraseelan JG, Goncalves N, Oliveira SMD, Häkkinen A, and Ribeiro AS 2016 Dissecting the stochastic transcription initiation process in live Escherichia coli. *DNA Res* **23** 203-14.

[41] Neeli-Venkata R, Startceva S, Annila T and Ribeiro AS 2016 Polar Localization of the Serine Chemoreceptor of Escherichia coli is Nucleoid Exclusion-Dependent *Biophys. J.* **111** 2512–22

[42] Skarstad K, Boye E and Steen HB 1986 Timing of initiation of chromosome replication in individual *Escherichia coli* cells *EMBO J.* **5** 1711-17

[43] Stouf M, Meile JC and Cornet F FtsK actively segregates sister chromosomes in Escherichia coli *Proc. Natl. Acad. Sci. USA* **110** 11157–62

[44] Hadizadeh YN, Guet CC, Johnson RC and Marko JF 2012 Variation of the folding and dynamics of the Escherichia coli chromosome with growth conditions *Mol. Microbiol.* **86** 1318–33

[45] Gupta A, Lloyd-Price J, Neeli-Venkata R, Oliveira SMD, and Ribeiro AS 2014 In vivo kinetics of segregation and polar retention of MS2-GFP-RNA complexes in Escherichia coli *Biophys. J.* **106** 1928–37

[46] Neeli-Venkata R, Martikainen A, Gupta A, Gonçalves N, Fonseca J. and Ribeiro AS 2016 Robustness of the Process of Nucleoid Exclusion of Protein Aggregates in Escherichia coli *J. Bacteriol.* **198** 898–906

[47] Bednarska NG, Schymkowitz J, Rousseau F and Van Eldere J 2013 Protein aggregation in bacteria: the thin boundary between functionality and toxicity *Microbiology* **159** 1795–806

[48] Galli E, Midonet C, Paly E and Barre FX 2017 Fast growth conditions uncouple the final stages of chromosome segregation and cell division in Escherichia coli *PLOS Gen.* **13** e1006702

[49] Häkkinen A and Ribeiro AS 2016 Characterizing Rate Limiting Steps in Transcription from RNA Production Times in Live Cells. *Bioinformatics* **32** 1346-1352.

[50] Kandavalli VK, Tran H, and Ribeiro AS 2016 Effects of σ factor competition on the in vivo kinetics of transcription initiation in Escherichia coli. *BBA Gene Regulatory Mechanisms* **1859** 1281–1288.

[51] Taschner PEM, Huls PG, Pas E, and Woldringh CL 1988 Division Behavior and Shape Changes in Isogenic ftsZ, ftsQ, ftsA, pbpB, and ftsE Cell Division Mutants of Escherichia coli during Temperature Shift Experiments. *J. Bacteriol.* **170** 1533-40.

[52] Le Gall A, Cattoni DI, Guilhas B, Mathieu-Demazière C, Oudjedi L, Fiche J-B, Rech J, Abrahamsson S, Murray H, Bouet J-Y, and Nollmann M 2016 Bacterial partition complexes segregate within the volume of the nucleoid. *Nat Commun.* **7** 12107.

[53] Winkler J, Seybert A, König L, Pruggnaller S, Hasselmann U, Sourjik V, et al. 2010 Quantitative and spatio-temporal features of protein aggregation in Escherichia coli and consequences on protein quality control and cellular aging. *EMBO J* **29** 910–923.

[54] Vecchiarelli AG, Mizuuchi K, and Funnell BE 2012 Surfing biological surfaces: exploiting the nucleoid for partition and transport in bacteria. *Mol Microbiol* **86** 513–523.

[55] Reyes-Lamothe R, Tran T, Meas D, Lee L, Li AM, Sherratt DJ, and Tolmasky ME 2014 High-copy bacterial plasmids diffuse in the nucleoid-free space, replicate stochastically

and are randomly partitioned at cell division. *Nucleic Acids Res* **42** 1042–1051.

[56] Straight PD, Fischbach MA, Walsh CT, Rudner DZ, and Kolter R 2007 A singular enzymatic megacomplex from Bacillus subtilis. *Proc Natl Acad Sci USA* **104** 305–310.